

Nonanalytic enhancement of the charge transfer from adatom to one-dimensional semiconductor superlattice and optical absorption spectrum

Satoshi Tanaka,^{1,*} Sterling Garmon,² and Tomio Petrosky^{2,3,†}¹*Department of Physical Science, Osaka Prefecture University, Sakai 599-8531, Japan*²*The Center for Complex Quantum Systems, The University of Texas at Austin, Austin, Texas 78712, USA*³*International Solvay Institute for Physics and Chemistry, Code Postal 231, 1050 Brussels, Belgium*

(Received 29 November 2005; published 30 March 2006)

The charge transfer from an adatom to a semiconductor substrate of one-dimensional quantum dot array is evaluated theoretically. Due to the Van Hove singularity in the density of electron states at the band edges, the charge transfer decay rate is enhanced nonanalytically in terms of the coupling constant g as $g^{4/3}$. The optical absorption spectrum for the ionization of a core level electron of the adatom to the conduction band is also calculated. The reversible non-Markovian process and irreversible Markovian process in the time evolution of the adatom localized state manifest themselves in the absorption spectrum through the branch point and pole contributions, respectively.

DOI: [10.1103/PhysRevB.73.115340](https://doi.org/10.1103/PhysRevB.73.115340)

PACS number(s): 73.20.At, 73.21.Cd, 73.21.Fg, 78.67.Lt

I. INTRODUCTION

Thanks to recent advances in nanotechnology, various types of artificial low-dimensional semiconductor structures have been fabricated.¹ The quantum confinement of electrons in these structures greatly modifies the density of states of carriers resulting in complete different electronic and optical properties from the bulk system.^{2,3} Recently one-dimensional quantum wires and quantum-dot arrays have been manufactured in various ways,^{1,4} and the formation of one-dimensional minibands has been theoretically and experimentally investigated.⁵⁻⁷ It has been found that the Van Hove singularity of the density of state inherent with the one dimensionality causes a characteristic electronic transport.^{8,9}

In this paper, we consider the charge transfer between an adatom localized state and a one-dimensional miniband associated with a quantum wire or quantum-dot array. The charge transfer between an adatom and a substrate semiconductor has been extensively studied.¹⁰ We will show that the low dimensionality greatly modifies the charge transfer process from the adatom to the semiconductor quantum-dot array due to the singularity of the density of states. The physical situation we consider in this paper is shown in Fig. 1(a) where an adatom is attached to a semiconductor quantum-dot array surface (hereafter we simply call it a superlattice).

The charge transfer of an electron from adatom to the miniband of the superlattice is caused by the hybridization of the adatom wave function with the miniband which can be described by the bilinear coupling between the adatom localized state and the bound state of a single quantum dot in which the adatom is situated. The situation may be described by one-dimensional version of Newns-Anderson model which has been extensively used to investigate the charge transfer process between the adatom and the semiconductor substrate.^{10,11} As shown below, the one-dimensional Newns-Anderson model we consider here is equivalent to the Friedrichs Hamiltonian which we have investigated in our previous letter.¹²

In this recent letter we reported a vast increase in the decay rate of an excited dipole molecule traveling in an one-

dimensionally confined electromagnetic waveguide when the cutoff frequency of the waveguide is near the characteristic frequency of the dipole.¹² This vast increase is a direct consequence of a singularity in the density of photon states at the cutoff frequency. Due to this singularity, standard perturbation analysis breaks down and hence one cannot apply Fermi's golden rule to evaluate the decay rate in the vicinity of the singularity. We have shown that in this case the decay rate of the excited dipole depends nonanalytically as $g^{4/3}$ on the coupling constant g . In the present article, we report that the same nonanalytic enhancement of the decay rate (including the $g^{4/3}$ law) can be found in our system, despite the fact that the density of electron states of the miniband of the superlattice is different from the density of states of photon states in a waveguide.

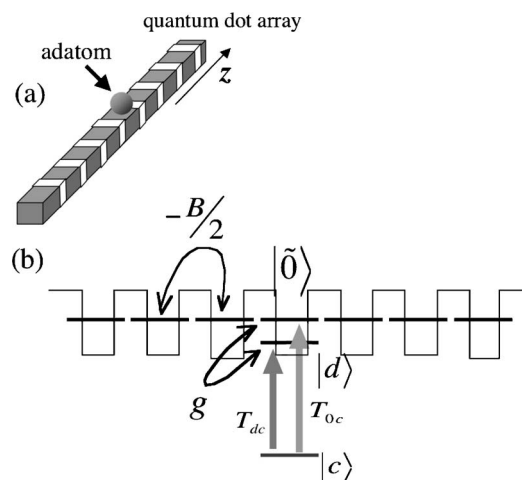


FIG. 1. (a) An adatom attached to a 1D quantum-dot array, and (b) level structures of the adatom localized state and the bound state in each quantum well. The width of each well is a few nm to 100 nm. The adatom is located at the $n=0$ th well. The two optical absorption transitions from the core level $|c\rangle$ with T_{dc} and T_{0c} are also shown by the arrows.

Although the exponential decay law for the unstable state has been observed ubiquitously in nature, quantum mechanics predicts that there should be a deviation from the exponential decay law for the unstable state.¹³ It has been shown that, irrespective of any specific form for the interaction, the time evolution of the surviving amplitude of an unstable state deviates from the exponential law on short and long time scales due to the existence of the lower bound on the energy, i.e., the branch point effect. Wilkinson *et al.* have recently succeeded in measuring the branch point effect in supercooled sodium atoms,¹⁴ even though the time scale in which the deviation from the exponential decay law appears is very short. Thus separation of the pole and branch point effects in the time evolution of the unstable state is essential to our understanding of the decay process, as has been done for a system composed of an excited atom coupled to a radiation field.^{15,16} The separation of the two effects is also useful because the reversible non-Markovian process in the decay process (due to the branch point effect) is directly related to the quantum Zeno effect.¹⁷⁻²⁰

Our goal is to present an actual experimental method that enables us to separately evaluate the pole and branch point effects for the decay process of the unstable state in this system. In this article, we consider the optical absorption process in which a core electron of the adatom with discrete energy is transferred to the continuous conduction band. It will be shown here that the spectral shape is influenced by the Markovian process due to the pole effect and also by the non-Markovian process due to the branch point effect.

The Friedrichs model presented here is equivalent to that known as the Fano model which was originally developed to explain the absorption spectrum for the autoionization process in the He atom.²² It is well known that this absorption spectrum has an asymmetric spectral profiles due to quantum interference between different optical transition paths. The appearance of the quantum interference indicates that the quantum coherence, which is a source of the memory effect, plays a key role in the decaying process of the excited state. As will be shown in the present paper, since the branch point effect which accounts for the non-Markovian decaying process with a memory effect is intensified by the singularity in the density of states, the absorption spectral profile provides us with the information on the extent of the persistence of the quantum coherence in the decaying process.

In Sec. II we present the model and show the nonanalytic enhancement of the decay rate for the unstable state. We decompose the absorption spectrum into contributions from the pole and branch point effects in Sec. III. In Sec. IV we summarize our results and provide some discussion.

II. MODEL AND NONANALYTIC ENHANCEMENT OF DECAY RATE

We consider a one-dimensional (1D) semiconductor superlattice with an adatom on the surface, as shown in Fig. 1(a). The width of each potential well is a few nm to 100 nm. One can make this device, for example, with GaAs/GaAlAs heterostructures.^{1,5} The superlattice consists of $N \gg 1$ identical quantum wells, and each well is assumed to have a single

bound state $|\tilde{n}\rangle$ ($\tilde{n} = -N/2$ to $N/2$) of equal energy, where the tilde is used to distinguish the site representation from the wave number representation below. A miniband is formed in the superlattice due to the electron tunneling through the potential barrier.^{2,6,7,23} We assume only nearest neighbor tunneling occurs with a transition probability of $\frac{-B}{2}$. The 1D superlattice is then represented by the one-dimensional tight binding model, and we have a continuous miniband of width $2B$ in the limit of $N \rightarrow \infty$. In addition to the miniband we consider an adatom localized state $|d\rangle$ with energy E_0 ; we also consider an inner core level $|c\rangle$ with energy E_c . Both of these states are associated with the adatom impurity located at the $n=0$ site. The adatom localized state $|d\rangle$ is hybridized with the $|\tilde{0}\rangle$ state with coupling strength gB .

Taking $\hbar=1$ hereafter, the electronic Hamiltonian H_E is then written as

$$H_E = E_c|c\rangle\langle c| + E_0|d\rangle\langle d| - \frac{B}{2} \sum_{(m,n)} |\tilde{m}\rangle\langle\tilde{n}| + gB(|d\rangle\langle\tilde{0}| + |\tilde{0}\rangle\langle d|), \quad (1)$$

where $\langle\cdots\rangle$ means taking nearest neighbor sum in Eq. (1). By introducing the wave number representation

$$|k\rangle \equiv \frac{1}{\sqrt{N}} \sum_{n=-N/2}^{N/2} \exp[ikn] |\tilde{n}\rangle, \quad (2)$$

we can rewrite H_E in the form of the Friedrichs model

$$H_E = E_c|c\rangle\langle c| + E_d|d\rangle\langle d| + \sum_k E_k|k\rangle\langle k| + \frac{1}{\sqrt{N}} \sum_k gB(|d\rangle\langle k| + |k\rangle\langle d|), \quad (3)$$

where $E_k = -B \cos k$. Note that our Hamiltonian does not involve the so-called counterrotating term as in the case of matter-field interaction systems. Nevertheless this form is exact, since the number of electron cannot change through the interaction in the system. We impose periodic boundary conditions, leading to $k = \frac{2\pi j}{N}$, where j is an integer running from $\frac{-N}{2}$ to $\frac{N}{2}$. The energy dispersion relation gives a divergence in the density of states at either band edge,

$$\rho(E_k) = \frac{1}{\pi \sqrt{B^2 - E_k^2}}. \quad (4)$$

For the 1D Friedrichs model, the electronic Hamiltonian H_E is diagonalized in terms of the so-called Friedrichs solution which results in the spectral representation²¹

$$H_E = E_c|c\rangle\langle c| + \sum_{i=1}^2 E_i|\phi_i\rangle\langle\phi_i| + \sum_k E_k|\phi_k^F\rangle\langle\phi_k^F|, \quad (5)$$

where $|\phi_i\rangle$ ($i=1,2$) are two stable eigenstates with energies E_i , and $|\phi_k^F\rangle$ with energy E_k (where $|E_k| < B$) is given by

$$|\phi_k^F\rangle = |k\rangle + \frac{1}{\sqrt{N}} \frac{gB}{\eta^+(E_k)} \left(|d\rangle + \frac{1}{\sqrt{N}} \sum_{k'(\neq k)} \frac{gB}{E_k - E_{k'} + i\epsilon} |k'\rangle \right), \quad (6)$$

with

$$\begin{aligned} \frac{1}{\eta^+(z)} &= G_{dd}^+(z) \equiv \langle d | \frac{1}{(z - H_E)^+} | d \rangle \\ &= \frac{1}{\left[z - E_0 - \frac{1}{N} \sum_k \frac{g^2 B^2}{z - E_k} \right]^+}, \end{aligned} \quad (7)$$

and a positive infinitesimal ϵ . The Green function $G_{dd}^+(z)$ is analytically continued from the upper half complex E_k plane to the lower half plane. Here, we do not write explicit forms of $|\phi_i\rangle$, since we will not use them in this paper.²¹ In the limit of $N \rightarrow \infty$, the summation over the wave number turns to the continuous integral, and then the self-energy term in Eq. (7) reads

$$\begin{aligned} \Xi(z) &\equiv \frac{1}{N} \sum_k \frac{g^2 B^2}{z - E_k} \rightarrow \frac{1}{2\pi} \int_{-\pi}^{\pi} dk \frac{g^2 B^2}{z - E_k} \\ &= \int_{-B}^B dE_k \rho(E_k) \frac{g^2 B^2}{z - E_k} = \frac{g^2 B^2}{\sqrt{z^2 - B^2}}. \end{aligned} \quad (8)$$

By substituting the right-hand side of Eq. (8) into $\eta^+(z)$ and taking the square of the dispersion relation we obtain a quartic equation in z . From the form of the quartic equation, it is readily seen that the solutions are symmetric about the origin $E_0=0$. By applying the standard method for solving a quartic equation, one can find the explicit solutions of the dispersion equation $\eta^+(z)=0$. The solutions consist of the pole $z_d \equiv \bar{E}_0 - i\gamma$ of $G_{dd}^+(z)$ in the lower half complex plane in the second Riemann sheet corresponding to the unstable decaying state, and the poles on the real axis corresponding to the stable states, $E_i (i=1,2)$. For illustration, we plot in Fig. 2(a) \bar{E}_0 and E_i for $g=0.5$ as a function of $\frac{E_0}{B}$ with thick dashed and solid lines, respectively. For arbitrary E_0 , there always exist two stable solutions outside the electronic miniband. Note that there is a critical value E_γ at which the unstable state with imaginary part $\gamma \neq 0$ appears. The unstable state exists for all $|E_0| < E_\gamma$, as indicated by the arrows in Fig. 2(a). In Fig. 2(b) we plot the decay rate $\frac{\gamma}{B}$ of the unstable solution for $g=0.1$ as a function of $\frac{E_0}{B}$. The maximum value of $\gamma = \gamma_{max}$ occurs at $E_0 = \pm B$.

Since the explicit form of the full solution is complicated, we present an approximate calculation of the maximum value γ_{max} of γ at $\frac{E_0}{B} = \pm 1$ and the critical value E_γ of E_0 where the unstable solution appears. To estimate γ_{max} we put $E_0 = B$ in the dispersion equation. After a simple manipulation we obtain

$$\zeta = 1 + (-1)^{2/3} \frac{g^{4/3}}{(\zeta + 1)^{1/3}}, \quad (9)$$

where $\zeta \equiv \frac{z}{B}$. The zeroth order solution (for $g=0$) is $\zeta=1$. We use this as our starting point and solve iteratively to find

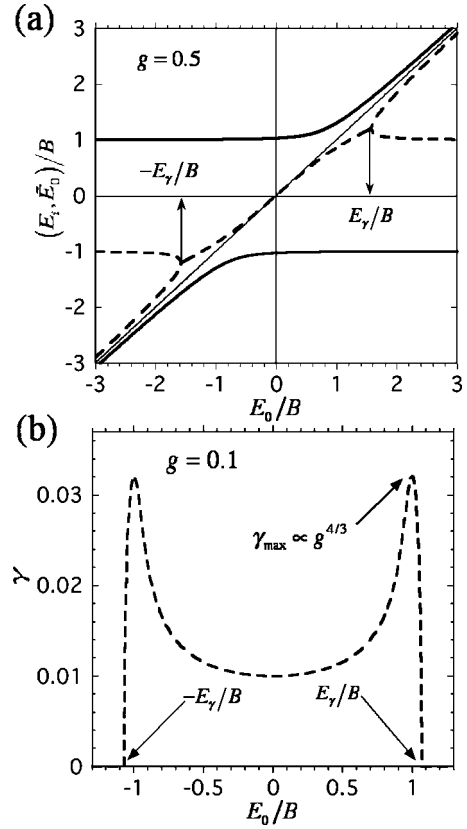


FIG. 2. (a) E_i/B and \bar{E}_0/B vs E_0/B for $g=0.5$, which are shown by the thick solid and dashed lines, respectively. The location of the critical values $\pm E_\gamma/B$ are indicated by the arrows. The thin line is $y=E_0/B$. (b) γ/B vs E_0/B for $g=0.1$. The maximum value of γ_{max}/B occurs at $E_0/B = \pm 1$.

$$\frac{\gamma_{max}}{B} = \frac{\sqrt{3}g^{4/3}}{2^{4/3}} + \frac{g^{8/3}}{2^{8/3}\sqrt{3}} + O(g^{16/3}), \quad (10)$$

where the third order contribution ($g^{4j/3}$ with $j=3$) vanishes.

To estimate E_γ near $E_0=B$ we put $z = E_0 + g^\alpha z_1$ where $\alpha > 0$ and z_1 are unknown variables which are independent of g . Then, by keeping only the predominant contribution to the dispersion equation, we obtain

$$\zeta - \bar{E}_0 \approx \frac{g^2}{\sqrt{\bar{E}_0 + 1} \sqrt{\zeta - 1}}, \quad (11)$$

where $\bar{E}_0 \equiv \frac{E_0}{B}$. Squaring this equation yields

$$f(\zeta) = (\zeta - \bar{E}_0)^2 (\zeta - 1) - \frac{g^4}{\bar{E}_0 + 1} \approx 0. \quad (12)$$

The function $f(\zeta)$ represents a cubic curve. By taking the derivative of $f(\zeta)$ and setting $f'(\zeta)=0$, we find the threshold value of $\bar{E}_0 = \frac{E_\gamma}{B} > 1$ at which the complex solutions of $f(\zeta)=0$ appear. This leads to the first two terms in the following expression for E_γ :

$$\frac{E_\gamma}{B} = 1 + \frac{3g^{4/3}}{2} - \frac{g^{8/3}}{8} + O(g^{12/3}). \quad (13)$$

For precision, we have presented the second order correction that is obtained from the exact solution of the original quartic equation. The values of γ and E_γ are nonanalytic in g for $g=0$, and hence one cannot obtain these results from a series expansion in g using ordinary perturbation analysis.

It should be noted that the $g^{4/3}$ law for the decay rate is rather universal around the edge of the continuous spectrum. Indeed, if the integration over the wave number in the self-energy is a Cauchy integral that is a double-valued function on z , as is the case in Eq. (7), then the edge of the miniband will give a square root type of essential singularity in the self-energy. In addition, if this singularity leads to a divergence at the edge, one can show that the $g^{4/3}$ effect appears in the vicinity of the singularity. Indeed, this is also the case for the dipole molecule traveling inside the waveguide mentioned above.¹²

In terms of the solutions of the dispersion equation obtained here, we may evaluate the time evolution of the surviving amplitude of the adatom localized state defined by $P(t) \equiv |\langle d | \exp[-iH_E t] | d \rangle|^2$. Indeed, aside from the persistent oscillation attributed to the two stable states, there are two contributions to the time evolution of the surviving amplitude; one comes from the pole contribution over the wave-number integral, where the location of the pole is given by the solution of the dispersion relation $\eta^+(E_k)=0$ in the complex E_k plane discussed above, and the other comes from the two branch point contributions that are located at the edges of the miniband at $\pm B$. As usual, the pole contribution leads to an exponential decay $\exp[-i(\tilde{E}_0 - i\gamma)t]$, while the branch point leads to a power law decay. If the condition $1 - \frac{|E_0|}{B} \gg g$ is satisfied, we have a well-separated time scale between the exponential and power law decay in the decay process of the localized state. The exponential law for the decay process is thus a good approximation for a time scale on the order of $t \sim \frac{1}{\gamma}$. However, once this condition is no longer fulfilled, the time separation becomes obscure and we must take into account the branch point effects in the time evolution. It is, however, a cumbersome task to evaluate the integral associated with the branch point in the time evolution. In the next section, we will evaluate the optical absorption spectrum instead, to separate the contribution of the Markovian effect from the non-Markovian effect. It should be generally easier in experiment to observe the absorption spectrum than a time evolution of the state $|d\rangle$.

III. ABSORPTION SPECTRUM

A. Spectral representation and the separation of the pole and branch point contributions

Here we consider the optical absorption by a transition from an inner core level of the adatom to the conduction electronic states of the 1D semiconductor superlattice, as shown in Fig. 1(b). There are two optical transition paths from the core level $|c\rangle$ with large transition amplitudes: One is that from the core level $|c\rangle$ to the localized state $|d\rangle$ and the

other is from the core level $|c\rangle$ to the $\tilde{n}=0$ site $|\tilde{0}\rangle$. The transition probabilities are denoted by T_{dc} and T_{0c} , respectively. The contributions of the transitions to the other bound states $|\tilde{n}\rangle$ are small, so we neglect the contributions in this paper, though it is not difficult to include those effects.

We consider here a single mode of the optical light field with frequency Ω . The total Hamiltonian is then written as

$$H_{total} = H_R + H_E + H_{RE}, \quad (14)$$

where the electronic Hamiltonian H_E is given in Eq. (3) and

$$H_R = \Omega a^\dagger a, \quad (15a)$$

$$H_{RE} = (T_{dc}|d\rangle\langle c| + T_{0c}|\tilde{0}\rangle\langle c|)a + \text{H.c.} \quad (15b)$$

$$\equiv \hat{T}a + a^\dagger \hat{T}^\dagger. \quad (15c)$$

The H_R represents a monochromatic light field where a (a^\dagger) is the annihilation (creation) operator of the field, and H_{RE} describes the interaction between the light field and the electronic system under the rotating wave approximation.

In the initial state of the absorption process, we have a core electron in the $|c\rangle$ state and a single photon with energy Ω ; we write this initial state as $|c; 1\rangle$ with energy $E_c + \Omega$, where 1 denotes the photon number for the mode Ω . After the absorption process the energy of the photon is transferred to the electronic system. The final states then take the form $|\phi_i; 0\rangle$ ($i=1, 2$) or $|\phi_k^F; 0\rangle$, with the energies E_i or E_k respectively.

When the value of $E_c + \Omega$ falls in between $-B$ and B , the state $|c; 1\rangle$ is resonant with the electronic continuum $|\phi_k^F\rangle$. As a result, the energy transfer from the light field to the electronic system occurs. Hereafter we take $-E_c$ as the origin of the light energy: $\Omega + E_c \rightarrow \Omega$.

The decay rate of $|c; 1\rangle$ is then determined by the pole location of the Green's function for $|c; 1\rangle$ as

$$G_{cc}^+(z) \equiv \langle c; 1 | \frac{1}{[z - H_{total}]^+} | c; 1 \rangle. \quad (16)$$

The decay rate $\gamma_{abs}(\Omega)$ is a function of Ω , and thus we identify the absorption spectrum as $F(\Omega) \equiv \gamma_{abs}(\Omega)$. In the weak coupling limit of T_{dc} and T_{0c} , the absorption spectrum $F(\Omega)$ reduces to

$$F(\Omega) = - \lim_{\epsilon \rightarrow 0^+} \text{Im} \sum_k \frac{|\langle \phi_k^F | \hat{T} | c \rangle|^2}{\Omega - E_k + i\epsilon} \quad (17a)$$

$$= - \lim_{\epsilon \rightarrow 0^+} \text{Im} \sum_k \frac{|\langle \phi_k^F | (T_{dc}|d\rangle + T_{0c}|\tilde{0}\rangle) |^2}{\Omega - E_k + i\epsilon}. \quad (17b)$$

The matrix element in Eqs. (17) may be obtained by using Eq. (6),

$$\langle d | \phi_k^F \rangle = \frac{gB}{\sqrt{N}} \frac{1}{\eta^+(E_k)} \quad (18a)$$

$$\begin{aligned} \langle \tilde{0} | \phi_k^F \rangle &= \frac{1}{\sqrt{N}} \left[1 + \frac{\Xi^+(E_k)}{\eta^+(E_k)} \right], \\ &= \frac{1}{\sqrt{N}} \frac{(E_k - E_0)}{\eta^+(E_k)}, \end{aligned} \quad (18b)$$

where the self-energy $\Xi^+(z)$ is give in Eq. (8).

Substituting Eqs. (18) into Eq. (17b), we then have

$$\begin{aligned} F(\Omega) &= -\text{Im} \frac{1}{N} \sum_k \frac{1}{\Omega - E_k + i\epsilon} \frac{1}{\eta^+(E_k) \eta^-(E_k)} \\ &\times \left[T_{dc}^2 + T_{0c}^2 \frac{(E_k - E_0)^2}{g^2 B^2} + 2T_{dc} T_{0c} \frac{(E_k - E_0)}{gB} \right], \end{aligned} \quad (19)$$

where $\eta^-(z)$ is analytically continued from the lower half plane. As done in Eq. (8), transforming the summation over the wave number into the integral in the limit of $N \rightarrow \infty$, the explicit form of $F(\Omega)$ is obtained as

$$\begin{aligned} F(\Omega) &= \frac{g^2 B^2 \sqrt{B^2 - \Omega^2}}{(B^2 - \Omega^2)(\Omega - E_0)^2 + g^4 B^4} \\ &\times \left[T_{dc}^2 + T_{0c}^2 \frac{(\Omega - E_0)^2}{g^2 B^2} + 2T_{dc} T_{0c} \frac{(\Omega - E_0)}{gB} \right]. \end{aligned} \quad (20)$$

Now we shall decompose the absorption spectrum $F(\Omega)$ into the pole and the branch point contributions. For this purpose, we first rewrite $F(\Omega)$ in terms of the contour integral by using the relation

$$\begin{aligned} \frac{1}{2\pi} \int_{-\pi}^{\pi} dk \dots &= \int_{-B}^B dE_k \rho(E_k) \dots \\ &= \frac{1}{2\pi i} \int_{-B}^B dE_k \frac{1}{g^2 B^2} [\eta^+(E_k) - \eta^-(E_k)] \dots, \end{aligned} \quad (21)$$

where... represents a function of k . By taking the limit of $N \rightarrow \infty$ and applying these relations to Eq. (19), $F(\Omega)$ may be cast into the form of a contour integral,

$$F(\Omega) = \text{Im} \frac{1}{2\pi i} \int_{\Gamma} \frac{1}{\Omega - E_k + i\epsilon} \frac{1}{\eta(E_k)} dE_k, \quad (22)$$

where the contour Γ is shown in Fig. 3(a). As shown in Fig. 3, the contour Γ can be deformed to that shown in Fig. 3(b), where the cross denotes the pole location at $E_k = z_d = \bar{E}_0 - i\gamma$. Along Γ , the solid and dashed lines are in the first and second Riemann sheets, respectively, so that $\eta(E_k)$ takes the corresponding value of $\eta^+(E_k)$ and $\eta^-(E_k)$ in Eq. (22), respectively.

In order to extract the pole contribution from Eq. (22), we evaluate the residue around the pole, and obtain

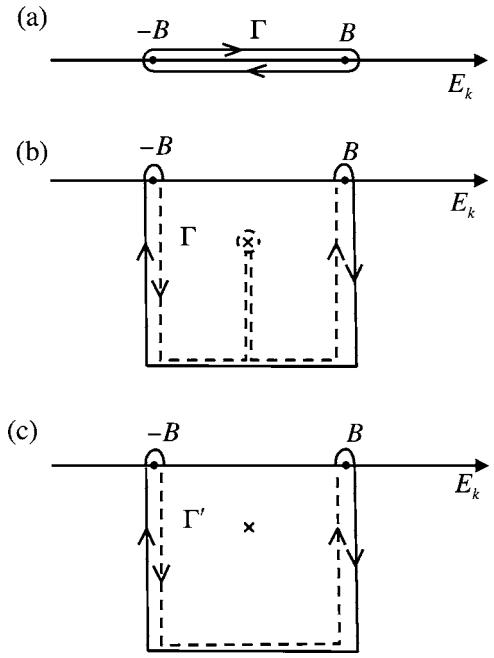


FIG. 3. The contours of the integral for $F(\Omega)$ Eq.(22) (a) and its deformation (b), and the integral for $F_0(\Omega)$ Eq. (23a) (c).

$$\begin{aligned} F_0(\Omega) &= \text{Im} \frac{1}{2\pi i} \int_{\text{pole}} dE_k \frac{1}{\Omega - E_k + i\epsilon} \frac{g^2 B^2}{\eta^+(E_k)} \\ &\times \left[T_{dc}^2 + T_{0c}^2 \frac{(\Omega - E_0)^2}{g^2 B^2} + 2T_{dc} T_{0c} \frac{(\Omega - E_0)}{gB} \right] \end{aligned} \quad (23a)$$

$$= -\text{Im} \frac{N_d}{\Omega - z_d} \left[T_{dc}^2 + T_{0c}^2 \frac{(z_d - E_0)^2}{g^2 B^2} + 2T_{dc} T_{0c} \frac{(z_d - E_0)}{gB} \right], \quad (23b)$$

where N_d is given by

$$N_d^{-1} = \frac{d}{dz} \left[z - E_0 - \frac{g^2 B^2}{N} \sum_k \frac{1}{(z - E_k)^+} \right]_{z=z_d} \quad (24a)$$

$$= 1 + \frac{z_d(z_d - E_0)}{z_d^2 - B^2}. \quad (24b)$$

Subtracting the pole contribution from Eq. (22), we can write the branch point contribution as

$$F_1(\Omega) = \text{Im} \frac{1}{2\pi i} \int_{\Gamma'} dE_k \frac{1}{\Omega - E_k + i\epsilon} \frac{1}{\eta(E_k)}, \quad (25)$$

where the contour Γ' is depicted in Fig. 3(c). The total absorption spectrum is then decomposed to $F(\Omega) = F_0(\Omega) + F_1(\Omega)$.

Though the exponentially decaying unstable state corresponding to the pole in the second Riemann sheet cannot be identified in the Hilbert space, it is possible to identify it outside the Hilbert space. One of the authors (T.P.) *et al.* have shown that the Friedrichs solution can be decomposed

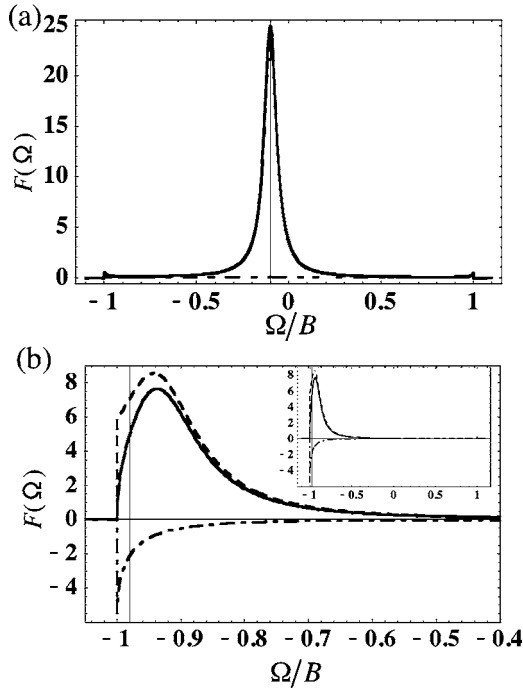


FIG. 4. The calculated $F(\Omega)$ (solid line), $F_0(\Omega)$ (dashed line), and $F_1(\Omega)$ (chain line) for $g=0.2$, and $T_{dc}=1.0$ and $T_{0c}=0$: (a) $E_0 = -0.1B$ and (b) $E_0 = -0.98B$. The thin vertical lines indicate the position of E_0 . In (b), the horizontal axis is expanded around $\Omega \approx -B$, while the overall spectrum is shown in the inset.

into the unstable state $|\phi_d\rangle$ (and $\langle\tilde{\phi}_d|$) and the dressed field states $|\phi_k\rangle$ (and $\langle\tilde{\phi}_k|$) in the generalized Hilbert space²⁴

$$\sum_k |\phi_k^F\rangle\langle\phi_k^F| = |\phi_d\rangle\langle\tilde{\phi}_d| + \sum_k |\phi_k\rangle\langle\tilde{\phi}_k|. \quad (26)$$

One can prove that this decomposition has one-to-one correspondence with the F_0 and F_1 spectral components. It should be noted that the factor N_d in Eqs. (24) is now recognized as a normalization constant of the unstable decaying state so that $\langle\tilde{\phi}_d|\phi_d\rangle=1$, and then $N_d = \langle d|\tilde{\phi}_d\rangle\langle\phi_d|d\rangle$.

B. Fano profile

In order to clarify the enhancement of the branch point effect due to the singularity of the density of states in the absorption spectrum, we first show in Fig. 4 the calculated results for an artificial situation with $T_{0c}=0$. We take $B=1.0$ and $T_{dc}=1.0$ in all calculations in the present work. In Fig. 4, the results for $g=0.2$ are shown for (a) $E_0=-0.1$ and (b) $E_0=-0.98$. Solid lines are the total absorption $F(\Omega)$ calculated by Eq. (20), while the dashed and the chain lines are the pole contribution $F_0(\Omega)$ in Eq. (23b) and the branch point contribution $F_1(\Omega)$ in Eq. (25), respectively. In Fig. 4(b), the spectra are magnified around $\Omega \approx -B$, while the overall spectrum is shown in the inset.

When $1 - \frac{|E_0|}{B} \gg g$ [Fig. 4(a)], the pole contribution $F_0(\Omega)$ is dominant in $F(\Omega)$; the $F_1(\Omega)$ contribution is very small except for the tiny increase around the band edges. In this case, $N_d \approx 1$ and $|\tilde{E}_0 - E_0| \ll gB$ in Eq. (23b), resulting in a

sharp Lorentzian spectrum of $F_0(\Omega)$ as shown in Fig. 4(a). The fact that $F_0(\Omega)$ is dominant in the entire energy region of $-B \leq \Omega \leq B$, suggests that the time evolution of the atom localized state almost completely obeys the exponential decay law, i.e., the Markovian process is predominant, as mentioned in the end of the previous section.

As E_0 gets close to the band edge [Fig. 4(b)], the decay rate of the unstable state is nonanalytically enhanced (as discussed in Sec. II) and the energy shift of $|\tilde{E}_0 - E_0|$ becomes large due to the singularity in the density of states of the miniband at the band edges, as shown in Fig. 2. Therefore the spectral width of $F_0(\Omega)$ gets wider and the shift of the peak position from E_0 becomes visible as shown in Fig. 4(b). Furthermore, it is found from Eq. (24b) that the divergence in the density of states enhances the second term in Eq. (24b), and thus N_d is largely reduced from 1 while $\text{Im}[N_d]$ remains negligibly small. Consequently, the relative ratio of the branch point contribution of $F_1(\Omega)$ to the pole contribution $F_0(\Omega)$ becomes larger than in Fig. 4(a). As discussed at the end of the previous section, the relative increase of the branch point contribution indicates that the time separation between the exponential and the power law decays becomes obscure in the time evolution of the surviving amplitude. Therefore, the non-Markovian process with memory effect becomes significant, which maintains the quantum coherence in the decaying process. The reduction of $N_d (= \langle d|\tilde{\phi}_d\rangle \times \langle\phi_d|d\rangle)$ also indicates that the unstable state $|\phi_d\rangle$ (or $\langle\tilde{\phi}_d|$) contains a larger contribution from the electronic continuum components of $|k\rangle$. This suggests that the contribution of the continuum to the dressing cloud is more significant. As shown below, the persistence of quantum coherence in the decay process, or the large dressing effect, manifests the quantum interference between the different optical transition paths once the other absorption transition T_{0c} is introduced.

Next we consider the actual case in which both optical transition paths are allowed: $T_{0c} \neq 0$ and $T_{dc} \neq 0$. We show in Fig. 5(a) the calculated results of $F(\Omega)$ for the same parameters as in Fig. 4(a) except that $T_{0c}=1.0$ here. The pole contribution $F_0(\Omega)$ and the branch point contribution $F_1(\Omega)$ are shown in Figs. 5(b) and 5(c), respectively. All these spectra are depicted by the solid lines. In each panel, the spectra are further decomposed into the spectral components due to the first, second, and the third terms in [...] of Eq. (20) or Eq. (23b). These terms are attributed to the d - d diagonal component, $\tilde{0}$ - $\tilde{0}$ diagonal component, and the interference term between these two in Eq. (17b). These are shown by the broken, dotted, and chain lines, respectively.

Introduction of T_{0c} changes the symmetric Lorentzian spectral shape of $F(\Omega)$ shown in Fig. 4(a), and yields an asymmetric spectral shape around $\Omega \approx E_0$ shown by the solid line in Fig. 5(a). As seen from Fig. 5(a), this is caused by the interference term of Eq. (20) shown by the chain line in the figure. Around $\Omega \approx \pm B$ the $F(\Omega)$ shows a sharp rise which reflects the divergence in the density of states, though $F(\Omega)$ remains finite around $\Omega \approx \pm B$ and $F(\pm B)=0$. It can be seen in Fig. 5(b) that $F_0(\Omega)$ is the dominant contribution to $F(\Omega)$ for $\Omega \approx E_0$ and we see that the antisymmetric spectral shape of the interference component of $F_0(\Omega)$ (chain line) is the

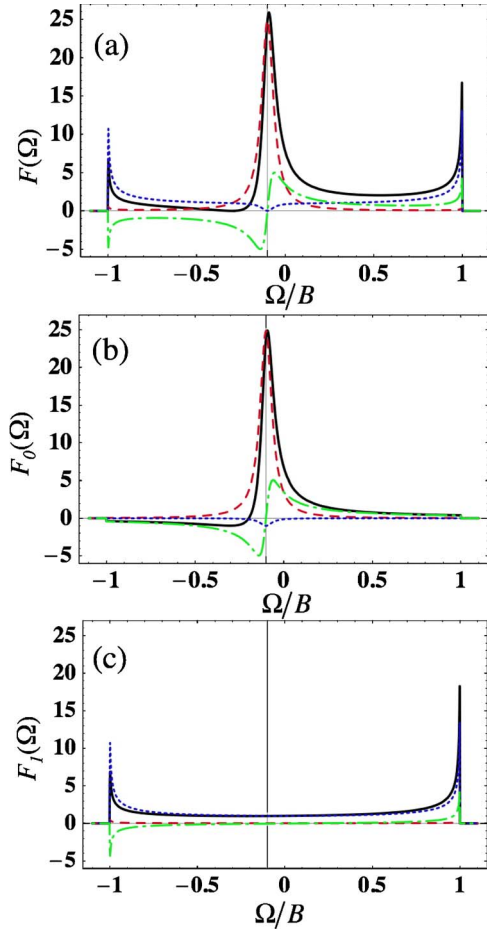


FIG. 5. (Color online) The calculated $F(\Omega)$ (a), $F_0(\Omega)$ (b), and $F_1(\Omega)$ (c) for the same parameters for Fig. 5(a) except $T_{0c}=1.0$: The spectra are decomposed into the d - d diagonal (dashed line), $\tilde{0}-\tilde{0}$ diagonal (dotted line), and the interference terms (chain line).

origin of the asymmetry in $F(\Omega)$. In fact, neglecting $\text{Im}[N_d]$ in Eqs. (23), which is appropriate except for $|E_0| > B$, the interference term in $F_0(\Omega)$ is approximately given by

$$F_0^{inter}(\Omega) = \frac{2T_{dc}T_{0c}}{gB} \text{Re}[N_d]\gamma \times \left\{ \frac{\Omega - \tilde{E}_0}{(\Omega - \tilde{E}_0)^2 + \gamma^2} + \frac{\tilde{E}_0 - E_0}{(\Omega - \tilde{E}_0)^2 + \gamma^2} \right\}. \quad (27)$$

When the condition $1 - \frac{|E_0|}{B} \gg g$ is satisfied, it holds that $\text{Re}[N_d] \approx 1$ and $\tilde{E}_0 - E_0 \ll 1$. As a result, only the first term of Eq. (27) contributes to F_0^{inter} [Fig. 5(b), chain line], leading to the antisymmetric spectral shape of the interference component of $F_0(\Omega)$. The asymmetric spectral shape obtained when the branch point effect is neglected is represented by the well-known Beutler-Fano profile.²²

However when E_0 lies close to the band edges, $|\tilde{E}_0 - E_0|$ becomes large, the second term of Eq. (27b) can no longer be neglected, which increases the interference component of $F_0(\Omega)$ compared to the d - d diagonal component. We show in

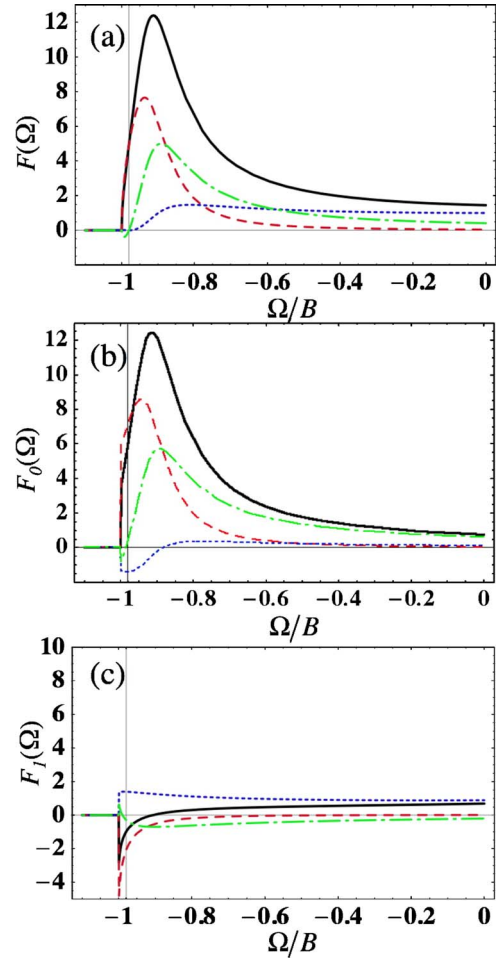


FIG. 6. (Color online) The parameters here are the same as in Fig. 5(b) except that $T_{0c}=1.0$.

Fig. 6 the calculated results for the same parameters as in Fig. 4(b) where $E_0 = -0.98B$, except that we take $T_{dc}=1.0$. As seen in Fig. 6(b) the interference component of $F_0(\Omega)$ (chain line) is enhanced compared with that in Fig. 5(b). As mentioned above, in this case quantum coherence plays a key role in the decay process, which is clearly reflected through the enhancement of the interference effect in the absorption spectrum.

IV. SUMMARY AND DISCUSSIONS

In the present work, we have evaluated the charge transfer rate from an adatom impurity on a 1D semiconductor superlattice. The decay rate is dramatically enhanced due to two square root forms of singularities in the density of states. In the vicinity of the singularities at either edge of the band spectrum, the decay rate becomes a nonanalytic function of the coupling constant g at $g=0$ as it can only be expanded in powers of $g^{4/3}$. The time evolution of the localized adatom state is governed by the pole and branch point contributions to the decay rate, which account for the exponential and nonexponential decay, respectively.

We have demonstrated that the absorption spectrum from the inner core level of the adatom to the conduction states is

an appropriate probe to observe both contributions. While the branch point effect is usually small, it becomes important when the adatom localized state is resonant with the miniband of the 1D superlattice in the vicinity of the singularity in the density of states. In the case where the branch point effect is significant, the quantum coherence in the decay process becomes exaggerated. This explains the enhancement of the quantum interference in the absorption spectrum.

The advantage of using the semiconductor superlattice is that it is easy to vary the parameters in an electronic system. Using modern nanotechnology, we can vary the parameter values widely, in order to systematically investigate the effect on the decay process. Other spectroscopic techniques, such as the resonant optical light scattering spectrum, may

also be used to investigate the time evolution of the unstable state in detail, which we are now studying.

ACKNOWLEDGMENTS

We thank V. Kocharovsky, G. Ordenez, W. Schieve, and G. Sudarshan for insightful discussions. We acknowledge the Engineering Research Program of the Office of Basic Energy Sciences at the U.S. Department of Energy, Grant No. DE-FG03-94ER14465 for supporting this work. This work was supported by the Grant-in-Aid for Scientific Research from the Ministry of Education, Science, Sports, and Culture of Japan.

*Electronic address: stanaka@p.s.cias.osakafu-u.ac.jp

†Electronic address: petrosky@physics.utexas.edu

¹R. Nötzel and K. H. Ploog, *Adv. Mater.* **5**, 22 (1993).

²S. E. Ulloa, E. Castano, and G. Kirczenow, *Phys. Rev. B* **41**, R12350 (1990).

³R. J. Haug, J. M. Hong, and K. Y. Lee, *Surf. Sci.* **263**, 415 (1992).

⁴M. S. Gudixsen, L. J. Lauhon, J. Wang, D. C. Smith, and C. M. Lieber, *Nature* **415**, 617 (2002).

⁵L. P. Kouwenhoven, F. W. J. Hekking, B. J. van Wees, C. J. P. M. Harmans, C. E. Timmering, and C. T. Foxon, *Phys. Rev. Lett.* **65**, 361 (1990).

⁶K. Nikolić and R. Sordan, *Phys. Rev. B* **58**, 9631 (1998).

⁷Y. S. Joe, D. S. Ikeler, R. M. Cosby, A. M. Satanin, and C. S. Kim, *J. Appl. Phys.* **88**, 2704 (2000).

⁸L. van Hove, *Phys. Rev.* **89**, 1189 (1953).

⁹A. Messica, A. Soibel, U. Meirav, A. Stern, H. Shtrikman, V. Umansky, and D. Mahalu, *Phys. Rev. Lett.* **78**, 705 (1997), D. Menashe and B. Laikhtman, *J. Phys.: Condens. Matter* **10**, 7793 (1998).

¹⁰*Surface Electron Transfer Processes*, edited by R. J. D. Miller (VCH, New York, 1995).

¹¹D. M. Newns, *Phys. Rev.* **178**, 1123 (1969).

¹²T. Petrosky, Chu-Ong Ting, and S. Garmon, *Phys. Rev. Lett.* **94**, 043601 (2005).

¹³L. A. Khal'fin, *Sov. Phys. JETP* **6**, 1053 (1958).

¹⁴S. R. Wilkinson, C. F. Bharucha, M. C. Fischer, K. W. Madison, P. R. Morrow, Q. Niu, B. Sundaram, and M. G. Raizen, *Nature* **387**, 575 (1997).

¹⁵G. Ordenez, T. Petrosky, and I. Prigogine *Phys. Rev. A* **63**, 052106 (2001).

¹⁶T. Petrosky, G. Ordenez, and I. Prigogine, *Phys. Rev. A* **64**, 062101 (2001).

¹⁷B. Misra and E. C. G. Sudarshan, *J. Math. Phys.* **18**, 756 (1977).

¹⁸W. M. Itano, D. J. Heinzen, J. J. Bollinger, and D. J. Wineland, *Phys. Rev. A* **41**, 2295 (1990).

¹⁹T. Petrosky, S. Tasaki, and I. Prigogine, *Physica A* **170**, 306 (1991).

²⁰K. Koshino and A. Shimizu, *Phys. Rep.* **412**, 191 (2005).

²¹K. Friedrichs, *Pure Appl. Math.* **1**, 361 (1948).

²²U. Fano, *Phys. Rep.* **15**, 1866 (1961).

²³Y. Zheng and T. Ando, *Phys. Rev. B* **66**, 085328 (2002).

²⁴T. Petrosky, I. Prigogine, and S. Tasaki, *Physica A* **173**, 175 (1991).